35th Annual International Conference of the IEEE EMBS
Osaka, Japan, 3 - 7 July, 2013

A Robust EC-PC Spike Detection Method for Extracellular Neural Recording

Yin Zhou and Zhi Yang

Abstract— **This paper models signals and noise for extracellular neural recording. Although recorded data approximately follow Gaussian distribution, there are slight deviations that are critical for signal detection: a statistical examination of neural data in Hilbert space shows that noise forms an exponential term while signals form a polynomial term. These two terms can be used to estimate a spiking probability map that indicates spike presence. Both synthesized data and animal data are used for the detection performance evaluation and comparison against other popular detectors. Experimental results suggest that the predicted spiking probability map is consistent with the benchmark and work robustly with different recording preparations.**

I. Introduction

Neurons in the brain form closely connected networks, where a most important information carrier is the action potential produced by individual neurons [1]–[3]. To capture action potentials and study information generation, representation, and propagation, they need to be extracted from the recorded data, referred to as spike detection. For *in vivo* neural recording experiments, reliable spike detection can be difficult. First, neurons are nonlinear, non-stationary devices which induce irregular, varied spike patterns [4], [5] coupled with interferences, artifacts, and noise. Second, it lacks labelled benchmark data for algorithm training. As a result, detection algorithms tend to be less specific and not adaptive to different recording conditions and data dynamics. Third, it is preferable to have detection algorithms that require less computational resources, thus feasible for hardware implementation. A low power, small area ASIC allows data compressed at the implant side and wirelessly transmitted to the external device.

In this paper, we report a novel EC-PC spike detection method for *in vivo* neural recording. It shows that neural data are a combination of two components by noise and detectable spikes. After Hilbert transform, the noise forms an exponential component (EC) and spikes form a polynomial component (EC). By using online trained EC and PC from raw data, the detector can output a spiking probability map that indicates the presence of spikes in a statistic manner. Compared with other approaches that assume tuned spike templates and stationary noise, or require careful adjustment of parameters, the proposed algorithm is nonparametric, self-adaptive, working reliably under different recording conditions. The EC-PC detection algorithm will be given first followed by experiments on both synthesized and animal data. Concluding remarks will be given the last.

Yin Zhou and Zhi Yang* are with ECE Department, National University of Singapore, Singapore, 119077. e-mail: {elezhouy,eleyangz}@nus.edu.sg. *Asterisk indicates corresponding author*

II. EC-PC spike detection algorithm

A. Noise vs. Spikes - EC/PC decomposition

Extracellularly recorded neural data consist of neural spikes (300Hz-5KHz), field potentials (<250Hz [6]) and noise (including other unresolved activities). After highpass filtering the data at 300Hz, recorded data are 1.) activities of neurons within the recording radius, where spike power is much stronger than the noise power, 2.) activities of neurons in an extended radius (up to a few hundred μm), where spike power is comparable to the noise power, and 3.) noise produced by different sources including unresolved synaptic activities, firing of distant neurons, and recording hardware.

To study both signals and noise in highpass filtered neural data, we refer to Central Limit Theorem (CLT) [7]: let X_i, $i = 1, 2, 3, ...K$ be a sequence of independent random variables. Suppose that each X_i has a finite expected value $E[X_i] = \mu_i$ and a finite variance $E[(X_i - \mu_i)^2] = \sigma_i^2$. If for some $\delta > 0$, the expected values $E[|X_i|^{2+2\delta}]$ are finite and the lyapunov's condition

$$\lim_{K\to\infty} \frac{1}{(\sum_{i=1}^{K} \sigma_i^2)^{1+\delta}} \sum_{i=1}^{K} E[|X_i - \mu_i|^{2+2\delta}] = 0 \quad (1)$$

is satisfied, then the convergence to Gaussian holds: $\sum_{i=1}^{K} X_i$ follows a Gaussian distribution with mean $\sum_{i=1}^{K} \mu_i$ and variance $\sum_{i=1}^{K} \sigma_i^2$.

Treating voltage fluctuation induced by individual neuronal source as a random variable (spike, synapse), the recorded data are the sum of many random variables with additional Gaussian noise by electrode interface and electronics. Due to the violations of Lyapunov's conditions, recorded neural data can be modeled as a mixture of Gaussian distribution by noise [8] and small amplitude activities from distant neurons ($> 100\mu m$) [9] and a second distribution by detectable spikes [10].

To simplify the computation and cater to ASIC implementation, Hilbert transform is used. Neural data sequence $V(t)$ and its Hilbert transform $HV(t)$ are related to each other that they together form a strong analytic signal $V_{st}(t)$ [11]

$$V_{st}(t) = V(t) + iHV(t) = V(t) + i\frac{1}{\pi} P \int_{-\infty}^{\infty} \frac{V(\tau)}{t-\tau} d\tau, \quad (2)$$

where P in front of the integral denotes the Cauchy principal value and H denotes Hilbert transform. Define

$$Z(t) = V_{st}(t)^2 \quad (3)$$

978-1-4577-0216-7/13/$26.00 ©2013 IEEE

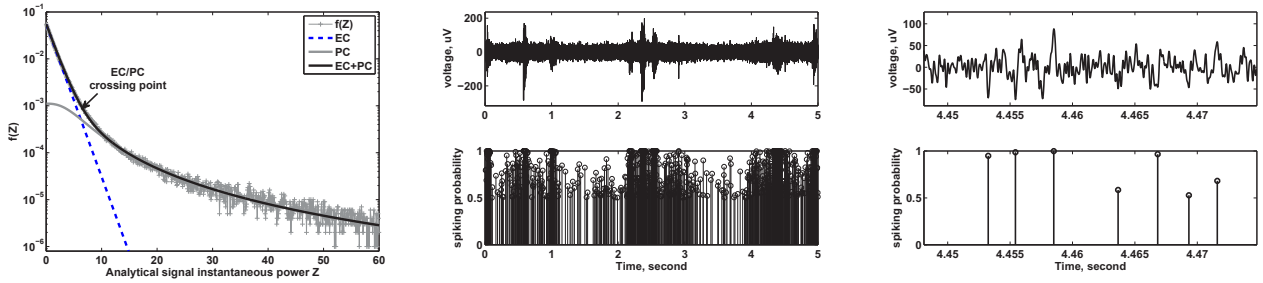

(a) (b) (c)

Fig. 1. (a) EC/PC decomposition. X-axis is the analytical signal power normalized to data variance; Y-axis is pdf. The figure shows the estimated EC (dashed blue), PC (solid grey) and superimposed EC+PC (solid black) in comparison with neural data distribution ($f(Z)$, dotted grey). (b) spiking probability map of a 5s *in vivo* data. Upper, bandpass filtered neural data. Bottom, corresponding spiking probability map with probabilities greater than 0.5 are plotted. X-axis is time and Y-axis the spiking probability. (c) Zoom-in figure at around 4.46s.

the instantaneous power of the analytic signal $V_{st}(t)$. For low SNR recordings e.g., no visually detectable spikes, the probability density function (pdf) $f(Z)$ is contributed by just noise and background activities which are Gaussian distributed. Therefore, $f(Z)$ follows χ^2 distribution with 2 degrees of freedom

$$f_n(Z) \approx \frac{1}{2\sigma^2} e^{-\frac{Z}{2\sigma^2}}, Z \geq 0, \tag{4}$$

where $f_n(Z)$ denotes noise probability density function and σ is the data standard deviation. From (4), $f_n(Z)$ has an exponential form, a straight line in the linear-log-scale.

For moderate and high SNR recordings, $f(Z)$ noticeable deviates from a straight line as shown in Fig. 1(a). To quantitatively investigate the second distribution, denote M the magnitude of a spike, by Coulomb's law, M is inversely proportional to the distance between the source (neuron) and the measuring point (electrode). Based on this property, the density function of the number of neurons with respect to M can be derived

$$\rho(M) = Cr(M)^2 |\frac{dr(M)}{dM}| \propto M^{-4}, \tag{5}$$

where C is a constant that relates to neuron density (the number of neurons per mm^3), $r(M)$ is the distance from a targeted neuron to the recording site.

To reach an analytical description, we assume individual analytic spikes introduce W equally spaced samples on average, based on (5), the added pdf by spikes to $f(Z)$ (the second distribution) is a polynomial component, as

$$f_d(Z) \approx [\int_s^{+\infty} \rho(M) \frac{W}{M} dM] \left. \frac{ds}{dZ} \right|_{s=Z^{0.5}} \propto \frac{1}{Z^{2.5}}.^{\mathbf{1}} \tag{6}$$

B. Spiking Probability of Neural Data Points

Equations (4) and (6) together suggest that $f(Z)$ is a combination of an exponential component (EC, $e^{-\lambda_1 Z}$, generated by noise) and a polynomial component (PC, $Z^{-\lambda_2}$, generated by spikes), as illustrated in Fig. 1(a). Assume $\widetilde{f_n}(Z)$ and $\widetilde{f_d}(Z)$ the exponential component and the polynomial component trained in real-time. Then the *"spiking probability"*, the probability that a data point with instantaneous power Z is from a spike, can be quantitatively assessed by

$$p(Z) = \frac{\widetilde{f_d}(Z)}{\widetilde{f_d}(Z) + \widetilde{f_n}(Z)} \approx \frac{\frac{b}{Z^{\lambda_2}+c}}{\frac{b}{Z^{\lambda_2}+c} + ae^{-\lambda_1 Z}}, \tag{7}$$

where {a,b} are the normalization coefficients that make $f(Z)$ sum to one and c is added to regulate PC at small Z thus prevents $f(Z)$ from going infinite. Specially, the data point Z satisfying $p(Z) = 0.5$ is defined as EC/PC crossing point, at which point spike power is equal to noise power and EC and PC curves in Fig. 1 cross each other. The square root of crossing point is denoted by $Z^{0.5}_{EC/PC}$. A typical plot of (7) as a function of Z is shown in Fig. 2.

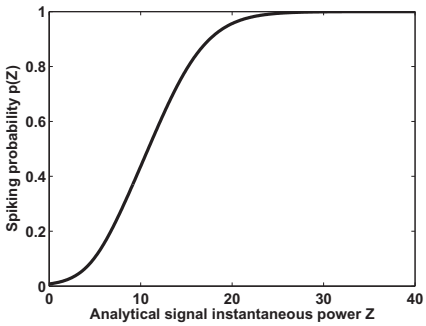

(a)

Fig. 2. A typical plot of analytical signal power Z vs. spiking probability p(Z) curve, according to (7).

In window detection, for an arbitrary time window $[m_i \Delta T, m_{i+1} \Delta T]$ of a few ms, we adopt a winner-take-all strategy. The probability that at lease one spike appears in the ith window is approximated by the peak spiking probability of the data points in the window:

$$P(i) = p(Z_i), Z_i = MAX\{Z(m\Delta T)\}, m_i \leq m < m_{i+1}. \tag{8}$$

[1]Equation. 5 and 6 have implicitly assumed that neural spike power is large than the noise power. As a result, when $f_d(Z)$ needs to be truncated when $Z < \sigma_n^2$.

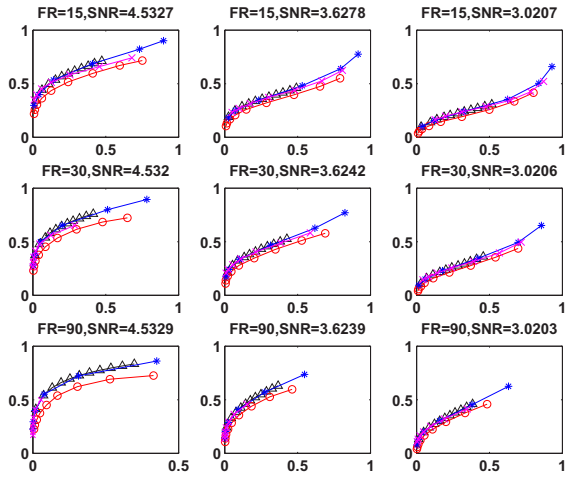

Fig. 3. ROC curves of four detection methods: EC-PC, black triangles; AT (absolute thresholding), blue stars; NEO, pink asterisks; CWD (continuous wavelet detector), red circles. The X-axis is probability of false alarm and Y-axis is probability of detection. Each curve is averaged from 100 trials. The evaluation is finished under low (15Hz), median (30Hz) and high (90Hz) firing rates (FR) and different noise levels. Each line shows the results with fixed firing rate and Each column represents the results with fixed noise levels.

A plotting of $P(i)$ over time is a predictive map of spikes and defined as *"spiking probability map"*, which is illustrated in Fig. 1(b) and (c). The probability applied on spiking probability map, ranging from 0 to 1, is defined as "probability threshold" in our proposed work.

III. Experiments on Synthesized Data

In this section, algorithm testing results on synthesized data are presented.

A. Data Preparation

Recorded *in vivo* data that contain a small number of visually detectable spikes are used as the background noise (20 - 30μV RMS) and extracted spike waveforms with large amplitude ($>$ 300μV) are used as spike templates. Up to 30 neurons are added within a few hundred μm radius of a point electrode, assuming a homogeneous neuron spatial distribution. The amplitude of each template is scaled inversely proportional to the distance between the electrode and space location of corresponding neuron. Individual neurons' firings are assumed to follow Poisson process with varied on/off firing states. The SNR in our experiments is defined as the averaged peak amplitude of spike templates over background noise RMS

$$SNR = \frac{\frac{1}{n}\sum_{i=1}^{n}|V_i|}{RMS_n}, \tag{9}$$

where V_i is peak amplitude of each spike template and RMS_n is noise RMS value.

B. Performance Comparison Against Other Techniques

In this section, the performance of EC-PC detector is evaluated and compared against three popular detectors.

- *Absolute Thresholding Detector (AT)*: spikes are detected when the absolute voltage exceeds a pre-determined threshold. The threshold is usually set w.r.t. to data RMS (root-mean-square of data amplitude) value. Here we sweep threshold from 2.5xRMS to 5xRMS with a step of 0.5xRMS.
- *NEO Detector (NEO)*: the output of NEO, $\psi[x(n)]$, is defined as $\psi[x(n)] = x^2(n) - x(n+1)x(n-1)$. The threshold for the NEO detector is set to be 5 to 11 times of the standard deviation of $\psi[x(n)]$.
- *Continuous Wavelet Detector (CWD)*: we choose *bior1.5* as mother wavelet, use 8 scales covering spike width from 0.5ms to 2ms and set the threshold from -0.2 to 0.2 as suggested by the authors [12].

The reason of choosing these three bench-marking detectors is mainly because they are from the amplitude based, the energy based and the spike shape based detection algorithms respectively which cover most widely used and discussed detectors. For the EC-PC detector, the probability threshold is set at 0.5-0.99 with a step of 0.05.

The quantitative evaluation is achieved by means of ROC curves as shown in Fig. 3. The X-axis is probability of false alarm (PFA) and Y-axis is probability of detection (PD) which are defined as

$$PD = \frac{N_{cd}}{N_a}, \; PFA = \frac{N_{fd}}{N_d}$$

where N_{cd},N_a,N_{fd} and N_d are the number of correctly detected spikes, total generated spikes, falsely detected spikes and total detected spikes. For all the detectors, a spike is seen to be correctly detected if it is within 0.5ms of the true arrival time given by ground truth data. The evaluation is finished under 9 combinations of different firing rates (15Hz, 30Hz and 90Hz) and SNRs (approximately 4.5, 3.6 and 3.0) with each repeated 100 times.

The threshold-averaged ROC curves [13] over 100 trials are shown in Fig. 3. The ROC curves show that no single detection method consistently outperforms the rests in all situations and the proposed EC-PC detector has a good performance in all the cases. Also note that different from AT and NEO, the EC-PC detector learns the data distribution and adaptively set threshold so that the probability of false alarm is less sensitive to the different recording situations, indicating a robust detection.

IV. Experiments on *in vivo* Data

In this section, we use *in vivo* data to further examine our work. We have designed a controlled experiment and the results are summarized in Fig. 4: a pair of microelectrodes are navigated into rat's brain to identify a recording location that gives sustained brain activities. After fixing the recording location, an anesthesia drug is injected to gradually stop the animal heart beating. As a result, neurons are dying because of lack of fresh blood. Continuous neural

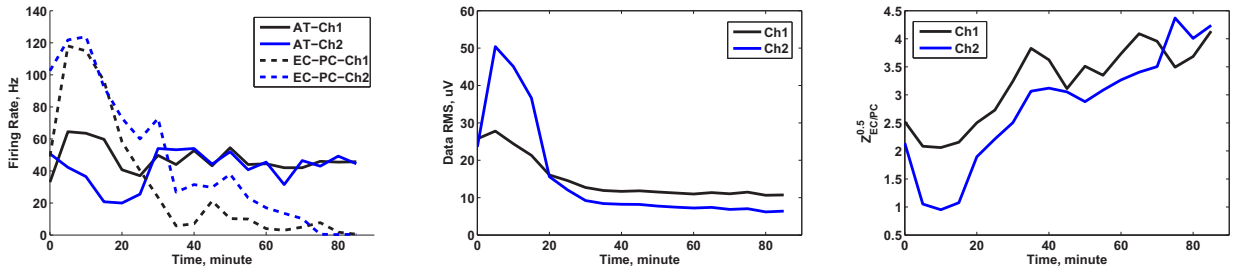

(a) (b) (c)

Fig. 4. (a) Estimated spike rate vs. time. The solid curves are obtained by setting the detection threshold at 3xRMS, while the dotted curves are read from the proposed spiking probability map. Blue and black traces are results from two separate electrodes. (b) Neural data RMS vs. time. X-axis is time in minute. Y-axis is data RMS in μV. The data have been bandpass filtered at 300Hz-5KHz. RMS estimation is performed every 5 minute. (c) Calculated EC/PC crossing point vs. time. Each crossing point is calculated based on 20 seconds data. Y-axis is EC/PC crossing point normalized to data RMS.

recordings at 25KHz/16b start from the electrode placement and last till the end of rat's life (data RMS reach a floor of around $10\mu V$). Spike detection and simple firing rate estimation is performed every 5 minutes using 20 seconds data. Fig. 4(a) plots estimated firing rates using both spiking probability map (dotted line) and amplitude thresholding detection with 3xRMS threshold(solid line). 3xRMS gives an almost constant firing rate during the subject dying period. As a comparison, the result from EC-PC detector with 0.8 probability threshold are more consistent with the experiment expectation to have spiking rate gradually decreasing and eventually to zero. Fig. 4(b) shows the RMS of the bandpass filtered data at 300Hz-6KHz, where the initial value is 25-$50\mu V$. Fig. 4(c) plots the $Z^{0.5}_{EC/PC}$ in RMS, which shows an increasing trend over time from 1 to 4 indicating that the spiking probability $p(Z)$ in Fig. 2 is moving towards right so the number of recorded spikes is decreasing. The result is not surprising because each time, EC-PC adaptively updates the coefficients of the neural data distribution. When animal's brain is dying, RMS of the recorded data is decreasing but the EC/PC crossing point $Z^{0.5}_{EC/PC}$ is actually increasing which leads to less detected events. This experiment shows that EC-PC detector is a good candidate of robust and unsupervised detectors.

V. Conclusion

We have reported a novel EC-PC spike detection algorithm. The basic idea of EC-PC spike detection is based on learning and fitting the data distribution. When transformed into Hilbert space, the Gaussian noise exhibits an exponential distribution while the deviation from exponential function, fitted by polynomial function, is resulted from the existence of detectable spikes. By curve fitting these two distributions, each recording setup or the different period in the same recording procedure, has specific coefficients to describe its characteristic. The detection performance of EC-PC detector is evaluated using both synthesized data and *in vivo* data. The results show that EC-PC detector is robust. Comparison result against other widely used detectors show that although no single detector outperforms the rest, the proposed EC-PC detector has a good performance in all the cases.

VI. Acknowledgement

This work is supported by Singapore A*STAR and MOE grants R-263-000-699-305, R-263-000-A32-305, R-263-000-A29-133, and R-263-000-619-133.

References

[1] J. Hopfield, "Pattern recognition computation using action potential timing for stimulus representation," *Nature*, vol. 376, no. 6535, pp. 33–36, Jul 1995.

[2] I. Stevenson and K. Kording, "How advances in neural recording affect data analysis," *Nature Neurosci.*, vol. 14, no. 22, pp. 139–142, Feb 2011.

[3] W. Gerstner, A. Kreiter, H. Markram, and A. Herz, "Neural codes: Firing rates and beyond," *Proc. Natl Acad. Sci.*, vol. 94, no. 24, pp. 12 740–12 741, Nov. 1997.

[4] M. Lewicki, "A review of methods for spike sorting: the detection and classification of neural action potentials," *Network: Computation in Neural Systems*, vol. 9, pp. 53–78, 1998.

[5] H. Kaneko, H. Tamura, and S. Suzuki, "Tracking spike-amplitude changes to improve the quality of multineuronal data analysis," *IEEE Trans. Biomedical Engineering*, vol. 54, no. 2, pp. 262–272, Feb 2007.

[6] A. Belitski, A. Gretton, C. Magri, Y. Murayama, M. A. Montemurro, N. K. Logothetis, and S. Panzeri, "Low-frequency local field potentials and spikes in primary visual cortex convey independent visual information," *J. Neurosci.*, vol. 28, no. 22, pp. 5696–5709, May 2008.

[7] P. Billingsley, "Probability and measure," *John Wiley sons*, 1995.

[8] S. Yu, H. Yang, H. Nakahara, S. Santos Gustavo, D. Nikolic, and D. Plenz, "Higher-order interactions characterized in cortical activity," *J. Neurosci.*, vol. 30, 2011.

[9] G. Buzsaki, C. A. Anastassiou, and C. Koch, "The origin of extracellular fields and currents - EEG, ECoG, LFP and spikes," *Nature Reviews Neuronsci.*, vol. 13, no. 6, pp. 407–420, Jun 2012.

[10] Z. Yang, W. Liu, M. R. Keshtkaran, Y. Zhou, J. Xu, V. Pikov, C. Guan, and Y. Lian, "A new EC-PC threshold estimation method for in vivo neural spike detection," *J. Neural Eng.*, vol. 9, no. 4, Aug. 2012.

[11] C. Schafer, M. Rosenblum, H. Abel, and J. Kurths, "Synchronization in the human cardiorespiratory system," *Physical Review E*, vol. 60, pp. 857–870, 1999.

[12] Z. Nenadic and J. Burdick, "Spike detection using the continuous wavelet transform," *IEEE Trans. Biomed. Eng.*, vol. 52, no. 1, pp. 74 –87, jan. 2005.

[13] T. Fawcett, "An introduction to ROC analysis," *Pattern Recognition Letters*, vol. 27, no. 8, pp. 861–874, Jun 2006.